iScience

CellPress
OPEN ACCESS

Article

Gasdermin D promotes hyperuricemia-induced renal tubular injury through RIG-I/caspase-1 pathway

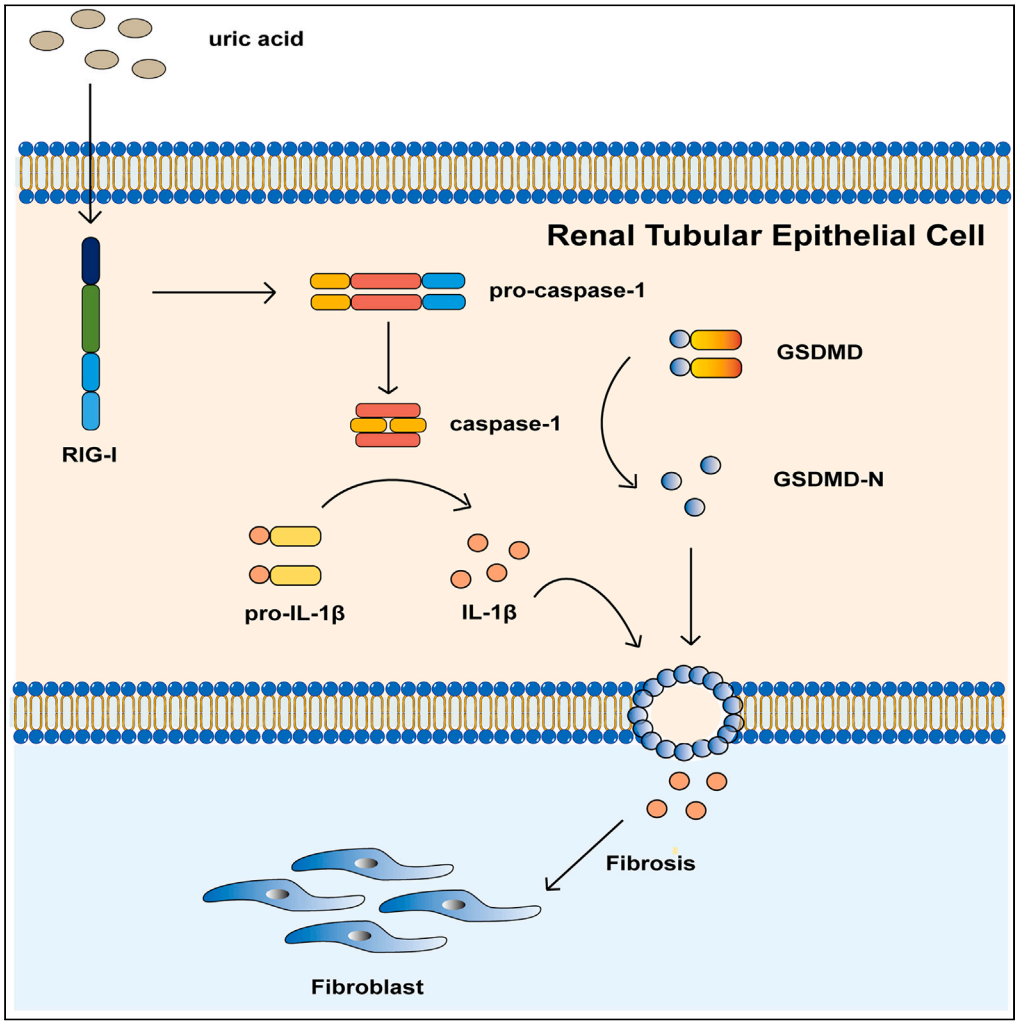

Lisha Ma, Ruiqin Shen, Jie Jiao, ..., Hao Luo, Limin Lu, Decui Shao

shaodecui@wnmc.edu.cn

Highlights

Genetic knockout GSDMD significantly improved hyperuricemia-induced renal injury

RIG-I physically interacts with caspase-1, RIG-I regulates caspase-1 activity

RIG-I/caspase-1/GSDMD pathway damages renal tubular epithelial cells with uric acid

Ma et al., iScience 26, 108463
December 15, 2023
https://doi.org/10.1016/j.isci.2023.108463

iScience

CellPress
OPEN ACCESS

Article

Gasdermin D promotes hyperuricemia-induced renal tubular injury through RIG-I/caspase-1 pathway

Lisha Ma,[1] Ruiqin Shen,[1] Jie Jiao,[1] Xiadong Lin,[1] Bin Zhai,[1] Aiping Xu,[1] Hao Luo,[1] Limin Lu,[2] and Decui Shao[1,3,*]

SUMMARY

Renal tubular epithelial cells injury is one of the most important pathological features in hyperuricemic nephropathy (HN). However, the involvement of gasdermin D (GSDMD)-mediated pyroptosis in HN remains obscure. We found GSDMD was upregulated in the kidney tissue of HN mice, which was accompanied by the loss of renal function, renal tubular fibrosis, and reduced body weight. These changes in HN mice were inhibited by GSDMD knockout. Knockdown of GSDMD inhibited the high uric acid-induced injury in cultured cells (NRK-52E). Mechanistically, co-immunoprecipitation showed that RIG-I exist in a complex with caspase-1. Overexpression of RIG-I induced increased expression of caspase-1 protein and caspase-1 activity. Caspase-1 interference significantly reduced the increase of caspase-1 activity and IL-1β production caused by RIG-I overexpression. Knockdown of RIG-I or caspase-1 decreased high uric acid-induced injury in NRK-52E. This work illustrates that targeting the RIG-I/caspase-1/GSDMD may provide potential therapeutic benefits to HN.

INTRODUCTION

Hyperuricemic nephropathy (HN) is a type of chronic kidney disease (CKD) caused by long-term hyperuricemia (HUA). HUA is recognized as an independent risk factor in CKD development, leading to abnormal serum uric acid levels, urate crystal deposition in renal tubules, changes in renal function and structure, and renal failure.[1] Therefore, identifying the exact mechanisms of kidney injury caused by HUA will help to develop new strategies for the treatment of HN.

As innate immune cells, renal tubular epithelial cells play a critical role in immunomodulation. Uric acid, a damage-associated molecular patterns (DAMPs), is a known agonist of the inflammasome through pattern recognition receptors (PRRs).[2] Recent studies have highlighted the involvement of inflammasome-mediated pyroptosis in various CKDs,[3–5] suggesting a potential role of pyroptosis in HUA-induced kidney injury. However, the precise mechanism by which uric acid triggers inflammation and renal tubular cell death remains unclear.

Caspase-1 is an inflammatory caspase that is activated through formation of inflammasome complexes in response to both pathogen-derived and endogenous mediators. The most well-known function of active caspase-1 is to cleave the preform of inflammatory cytokine IL-1β into its active forms in response to inflammatory stimuli in immune cells. Pyroptosis, a regulated cell death form, relies on gasdermin family proteins to cause plasma membrane pores. In classical pyroptosis pathways, inflammasomes recognize different infectious and injury factors and form inflammatory complexes with caspase-1.[6] A series of studies have shown that most inflammasomes and caspase-1 formations depend on apoptosis-associated speck-like protein containing CARD (ASC).[7,8] In addition, there are a type of NOD-like receptors embracing a caspase activation and recruitment domain (CARD), performing independently of ASC activation.[9]

Retinoic acid inducible gene-I (RIG-I), also known as DDx58, is a newly discovered PRR which localized in cytoplasm and nucleus, and RIG-I is the only DEAD/H-box protein containing CARD. Previous RIG-I studies have focused on infectious diseases, where activation of RIG-I leads to recruitment of mitochondrial antiviral signalings (MAVs), leading to induction of a type I interferon response.[10] However, recent studies have unveiled additional functions of RIG-I beyond its antiviral role, highlighting its significance in noninfectious diseases.[11,12] RIG-I exhibits close associations with the caspase family, particularly caspase-1/3/8/9, due to its N-terminal caspase recruitment domain.[13–15] Notably, Poeck H et al. demonstrated that RIG-I could activate and release IL-1β by recognizing RNA viruses.[16] Growing evidences indicated RIG-I was involved in the activation of caspase-1, triggering inflammation through pyroptosis. However, the role of RIG-I/caspase-1 signaling in HUA remains elusive.

Therefore, we established HUA mouse models and global knockout of gasdermin D (GSDMD) to investigate whether modulating GSDMD could alleviate kidney injury induced by HUA. Furthermore, we examined the RIG-I/caspase-1/GSDMD pathway in renal tubular epithelial cell lines.

[1]Cell Electrophysiology Laboratory, Wannan Medical College, 22 Wenchangxi Road, Wuhu 241002, China
[2]Department of Physiology and Pathophysiology, Shanghai Medical College, Fudan University, 138 Yixueyuan Road, Shanghai 200032, China
[3]Lead contact
*Correspondence: shaodecui@wnmc.edu.cn
https://doi.org/10.1016/j.isci.2023.108463

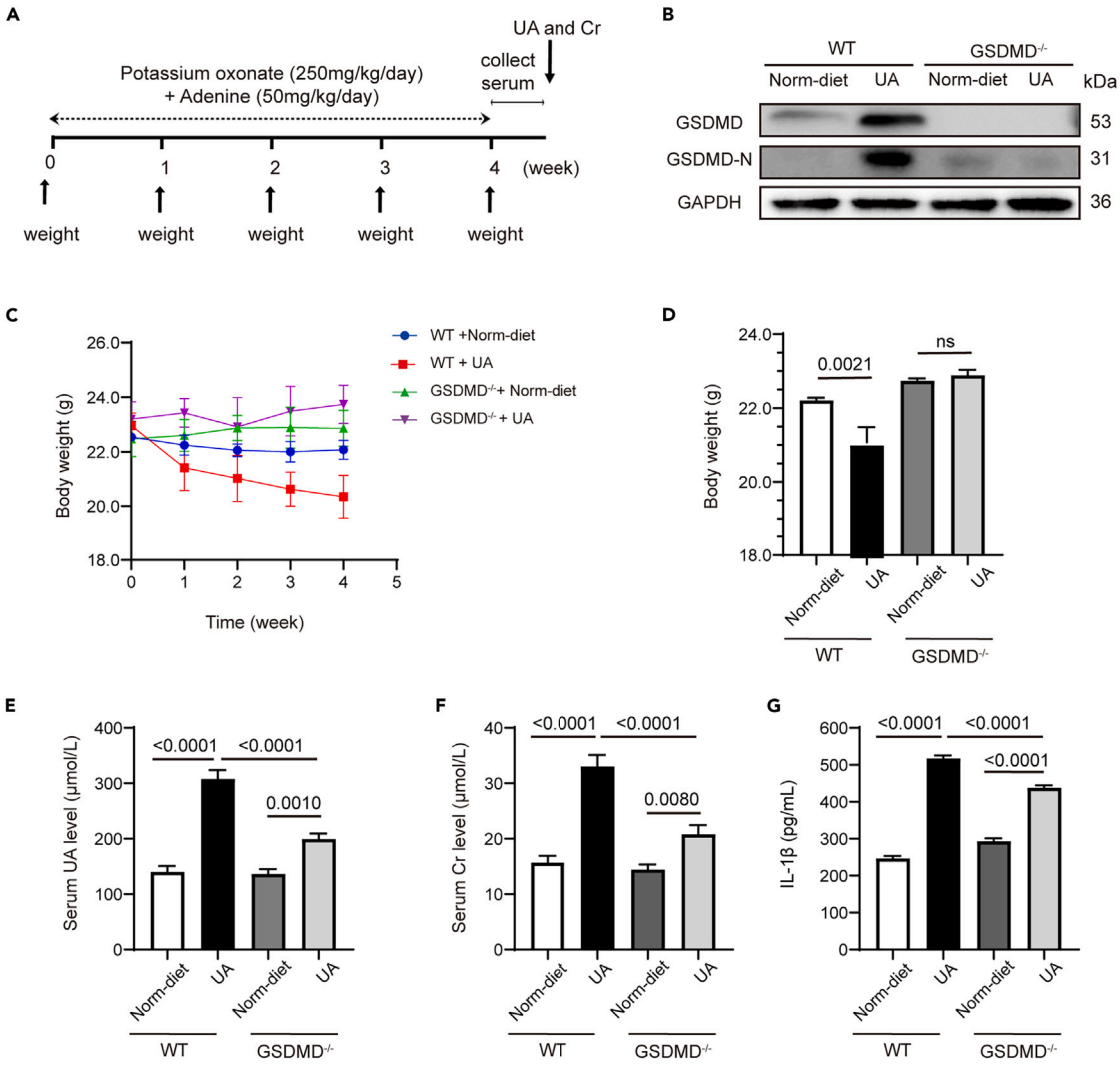

Figure 1. Successful establishment of the HN mice model induced by OXO/adenine in WT mice and GSDMD$^{-/-}$ mice

(A) The experimental design is presented schematically.

(B) Western blot showing GSDMD and GSDMD-N levels in renal tissue from the WT and GSDMD$^{-/-}$ mice.

(C and D) Body weight (BW) measurements were taken weekly, and the final BW was found to increase after OXO/adenine treatment (n = 6 animals per group).

(E and F) Serum UA (E) and Cr (F) levels in control and OXO/adenine-induced mice (n = 6 animals per group).

(G) IL-1β level in renal tissues (n = 6 animals per group).

Data for (C)-(G) are presented as mean ± SEM. One-way ANOVA with Student-Newman-Keuls test for (D–G). WT, wild type. Norm-diet, normal diet. UA, uric acid. Cr, creatinine.

RESULTS

Successful establishment of the HN mice model induced by OXO/adenine in WT mice and GSDMD$^{-/-}$ mice

GSDMD knockout (GSDMD$^{-/-}$) mice were used to judge GSDMD function in OXO/adenine-induced HUA in mice. Twenty-four mice (WT-Norm-diet, WT-HUA, GSDMD$^{-/-}$-Norm-diet and GSDMD$^{-/-}$-HUA) were used. To investigate the role of pyroptosis in HUA, we used an OXO/adenine-induced mouse model (Figure 1A). GSDMD and cleaved gasdermin D (GSDMD-N) proteins were hardly expressed in GSDMD$^{-/-}$ mice (Figure 1B). The body weight of mice in the WT-HUA group decreased rapidly, and knockdown of GSDMD attenuated the OXO/adenine-induced reduction in body weight (Figure 1C). At the end of the experiment, the body weight was not significantly different in GSDMD$^{-/-}$ mice with or without OXO/adenine treatment (Figure 1D). The serum uric acid (UA) levels significantly increased in response to OXO/Adenine treatment in both WT and GSDMD$^{-/-}$ mice, but the increase was lower in GSDMD$^{-/-}$ mice than in WT mice (Figure 1E). Additionally, GSDMD knockout alleviated renal injury induced by HUA, as indicated by the levels of serum creatinine, an important indicator of renal injury (Figure 1F). Furthermore, the upregulation of IL-1β expression observed in hyperuricemic mice was attenuated by GSDMD knockout (Figure 1G).

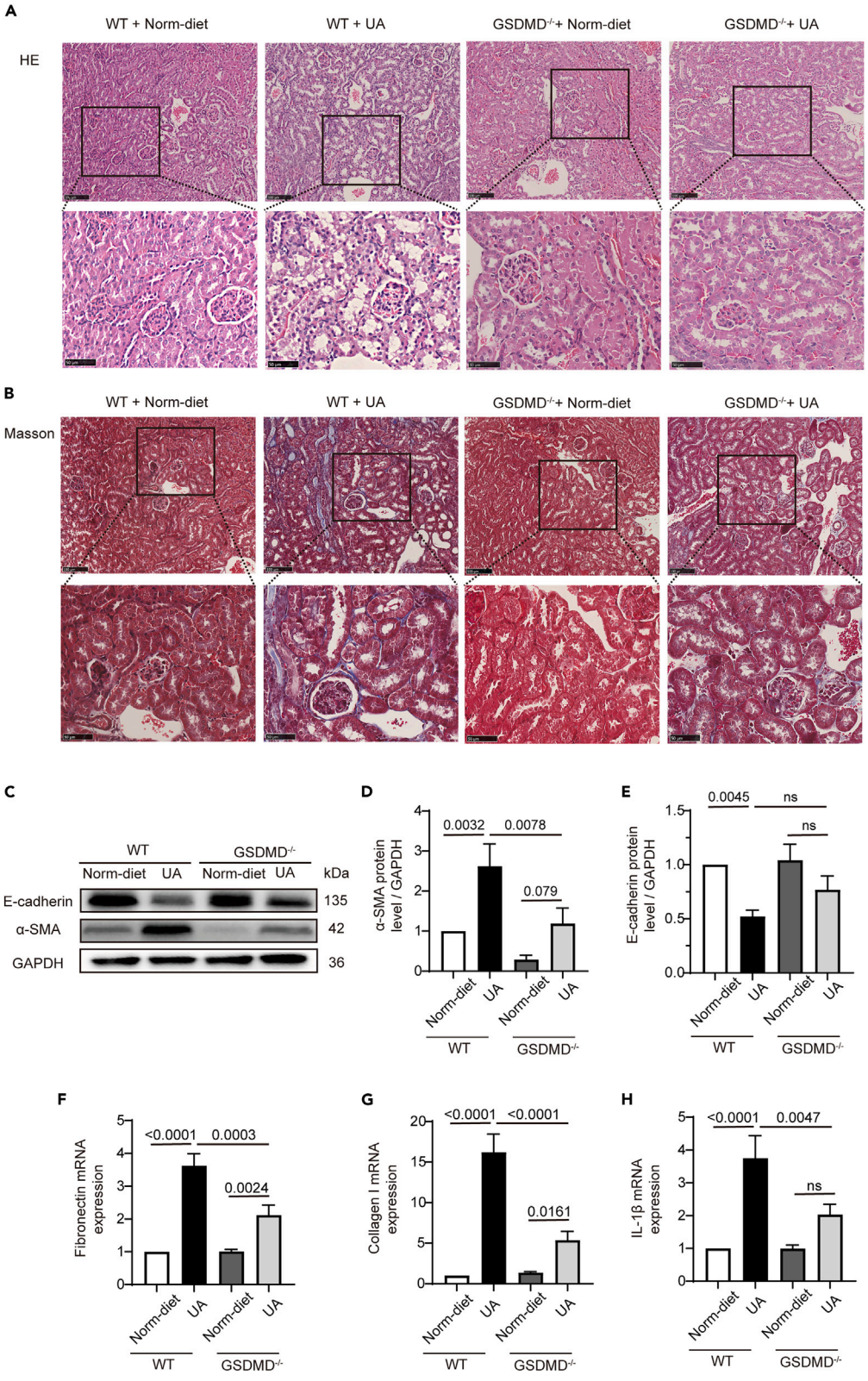
A
WT + Norm-diet
WT + UA
GSDMD-/-+ Norm-diet
GSDMD-/-+ UA
HE
B
WT + Norm-diet
WT + UA
GSDMD-/-+ Norm-diet
GSDMD-/-+ UA
Masson
C
WT
GSDMD-/-
Norm-diet
UA
Norm-diet
UA
kDa
E-cadherin
135
α-SMA
42
GAPDH
36
D
α-SMA protein level / GAPDH
0.0032
0.0078
0.079
Norm-diet
UA
Norm-diet
UA
WT
GSDMD-/-
E
E-cadherin protein level / GAPDH
0.0045
ns
ns
Norm-diet
UA
Norm-diet
UA
WT
GSDMD-/-
F
Fibronectin mRNA expression
<0.0001
0.0003
0.0024
Norm-diet
UA
Norm-diet
UA
WT
GSDMD-/-
G
Collagen I mRNA expression
<0.0001
<0.0001
0.0161
Norm-diet
UA
Norm-diet
UA
WT
GSDMD-/-
H
IL-1β mRNA expression
<0.0001
0.0047
ns
Norm-diet
UA
Norm-diet
UA
WT
GSDMD-/-

Figure 2. Knockout of GSDMD alleviated renal tubule morphological changes in OXO/adenine-induced mice and attenuated fibrosis

(A and B) Histological changes in renal tubules after HE (A) and Masson (B) staining in different groups. Scale bar 50 μm and 100μm.

(C and D) Western blot showing α-SMA levels in renal tissue from different groups (n = 6 animals per group).

(C and E) Western blot showing E-cadherin levels in renal tissue from different groups (n = 5 animals per group).

(F and G) RT−PCR analysis of fibronectin (F) and collagen I (G) levels in renal tissue from different groups (n = 5 animals per group).

(H) RT−PCR analysis of IL-1β levels in renal tissue from different groups (n = 6 animals per group).

Data for (D)-(H) are presented as mean ± SEM. One-way ANOVA with Student-Newman-Keuls test for (D–H). WT, wild type. Norm-diet, normal diet. UA, uric acid.

Knockout of GSDMD alleviated renal tubule morphological changes in OXO/adenine-induced mice and attenuated inflammation

HE staining showed that OXO/adenine-induced mice exhibited increased renal tubular cell vacuolation and lumen dilation. In OXO/adenine-induced GSDMD$^{-/-}$ mice, the above changes were ameliorated (Figure 2A). Masson staining was employed to assess renal tissue fibrosis, demonstrating that the WT-HUA group exhibited a larger area of fibrosis in renal tubules compared to other groups (Figure 2B). All histological analyses showed that pathomorphological and fibrotic changes in renal tubules were markedly ameliorated in OXO/adenine-induced GSDMD$^{-/-}$ mice.

Western blot analysis further showed that fibroblast marker (α-SMA) levels were increased by OXO/adenine induction, and epithelial-mesenchymal transition marker (E-cadherin) expression was reduced by OXO/adenine treatment. However, to some extent, knockout of GSDMD partially reversed OXO/adenine-induced renal fibrosis (Figures 2C–2E). Relative expression of fibronectin, collagen I and IL-1β gene expression detected by RT-PCR, the PCR primers are listed in Table 1. RT−PCR confirmed that the increasing levels of fibronectin, collagen I and IL-1β induced by OXO/adenine treatment were reversed in GSDMD$^{-/-}$ mice (Figures 2F–2H).

Hyperuricemia activated the RIG-I/caspase-1/GSDMD pyroptosis pathway in renal tubules

Clustered heatmap data for control and HN mice were obtained from the Gene Expression Omnibus (GEO:GSE190205). The heatmap shows that pyroptosis-related genes, fibrosis-related genes, and DDx58 were upregulated in mice with HN compared to control mice (Figure 3A). Furthermore, a potential interaction between RIG-I and caspase-1 was suggested based on recent studies, and a schematic diagram depicting the molecular structure of RIG-I and caspase-1, with the CARD as a possible interaction site, was presented (Figure 3B).

In line with these findings, western blot analysis of renal tissues showed elevated levels of cleaved-caspase-1, caspase-1, and RIG-I in mice administered with OXO/adenine intragastrically for 28 days, compared to the normal diet-fed group (Figures 3C–3F).

Water influx through aquaporin-1 (AQP-1) is used as a proximal tubular marker because of its high expression in the proximal tubule. Immunofluorescence results displayed that RIG-I and caspase-1 were expressed in the normal proximal tubule (Figures 3G and 3H). In addition, we also isolated mouse renal tubules and observed the expression of GSDMD in the primary renal tubules (Figure S1). Also, RIG-I co-localized with caspase-1 (Figure 3I). Those results suggested that RIG-I and caspase-1 may interact with each other in proximal tubule. Additionally, co-immunoprecipitation (Co-IP) assay in NRK-52E cells treated with uric acid for 48 h confirmed the interaction between RIG-I and caspase-1 at the protein level (Figure 3J).

GSDMD encouraged IL-1β expression and fibrosis in NRK-52E cells *in vitro*

To determine the influence of uric acid, HK-2 and NRK-52E cells were each stimulated with uric acid. In HK-2 cells, RIG-I, caspase-1 and GSDMD levels were measured and were significantly higher compared to the control cells (Figures 4A–4D). NRK-52E cells also showed a similar response (Figures 4E–4H).To further investigate the role of RIG-I, caspase-1 and GSDMD genes in renal tubular epithelial injury induced by uric acid, small interfering RNAs (siRNAs) were applied. Their sequences are shown in Table 2.

To determine the common effect of HUA in vivo and in vitro, GSDMD-specific siRNA was transfected into NRK-52E cells prior to uric acid treatment. The increase in GSDMD levels and GSDMD cleavage induced by uric acid was attenuated by knockdown of GSDMD expression, as

Table 1. The primer sequences used in RT−PCR

Gene name	Primer (5′ to 3′)
GAPDH	Sense: GGCAAATTCAACGGCACAGTCAAG
	Antisense: TCGCTCCTGGAAGATGGTGATGG
IL-1β	Sense: GCAACTGTTCCTGAACTCAACT
	Antisense: ATCTTTTGGGGTCCGTCAACT
Fibronectin	Sense: CGTCGGTCACTTCCACAAAC
	Antisense: GGAGAACCAGGAGAGCACAC
Collagen I	Sense: CAGGAGAACCAGGAGAACCAGGAG
	Antisense: GACAGGCGAACAAGGTGACAGAG

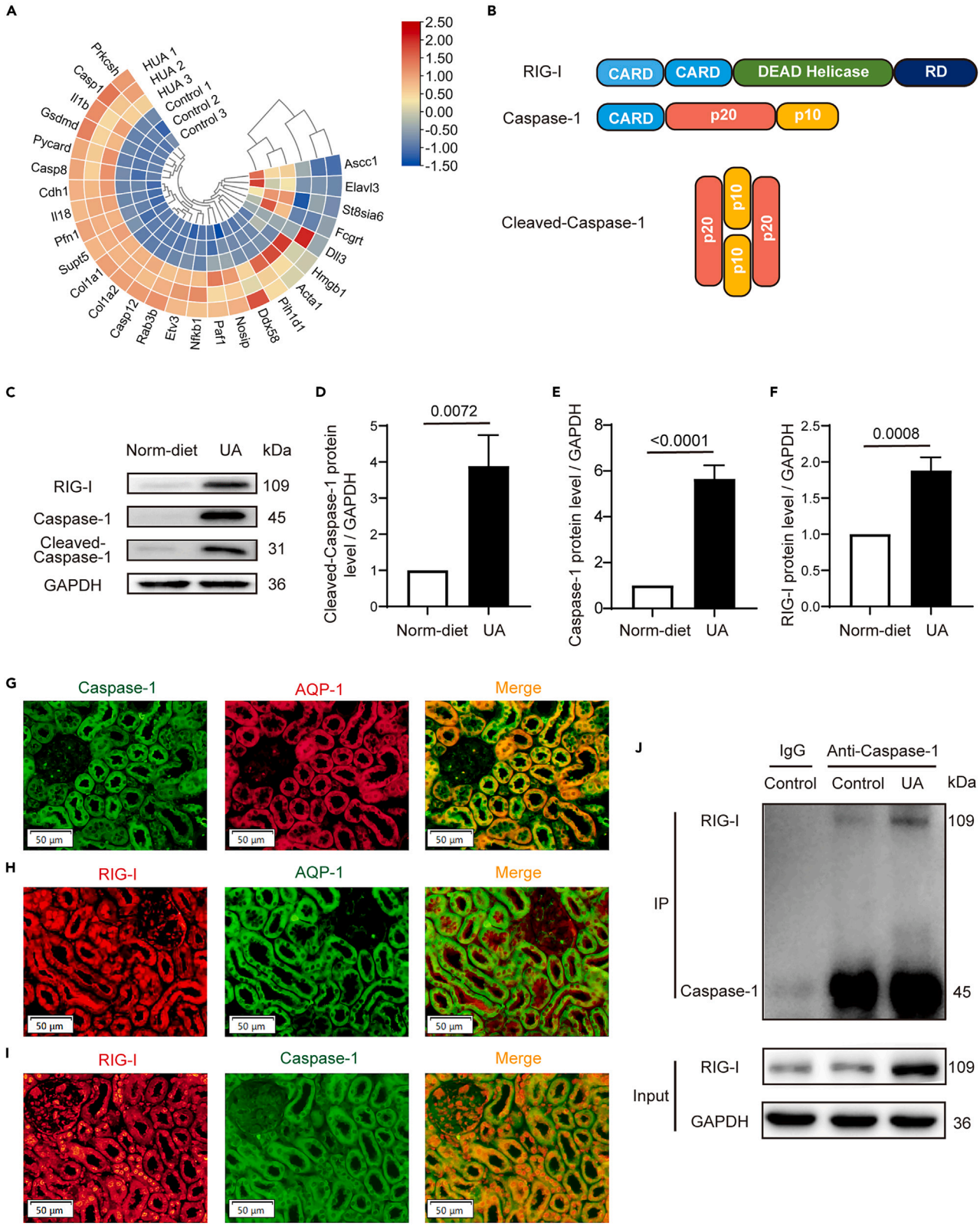
A
HUA 1
HUA 2
HUA 3
Control 1
Control 2
Control 3
Prkcsh
Casp1
Il1b
Gsdmd
Pycard
Casp8
Cdh1
Il18
Pfn1
Supt5
Col1a1
Col1a2
Casp12
Rab3b
Etv3
Nfkb1
Paf1
Nosip
Ddx58
Pih1d1
Acta1
Hmgb1
Dll3
Fcgrt
St8sia6
Elavl3
Ascc1
2.50
2.00
1.50
1.00
0.50
0.00
-0.50
-1.00
-1.50
B
RIG-I
CARD
CARD
DEAD Helicase
RD
Caspase-1
CARD
p20
p10
Cleaved-Caspase-1
p20
p10
p10
p20
C
Norm-diet
UA
kDa
RIG-I
109
Caspase-1
45
Cleaved-Caspase-1
31
GAPDH
36
D
0.0072
Cleaved-Caspase-1 protein level / GAPDH
Norm-diet
UA
E
<0.0001
Caspase-1 protein level / GAPDH
Norm-diet
UA
F
0.0008
RIG-I protein level / GAPDH
Norm-diet
UA
G
Caspase-1
AQP-1
Merge
50 μm
H
RIG-I
AQP-1
Merge
50 μm
I
RIG-I
Caspase-1
Merge
50 μm
J
IgG
Anti-Caspase-1
Control
Control
UA
kDa
IP
RIG-I
109
Caspase-1
45
Input
RIG-I
109
GAPDH
36

Figure 3. HUA activated the RIG-I/caspase-1/GSDMD pyroptosis pathway in renal tubules

(A) Clustered heatmap of the relative proteins in HN (n = 3 animals per group). The color scale from blue (reduction) to white (low intensity) to red (increases).

(B) Schematic diagram of RIG-I and caspase-1 molecular structure.

(C–F) Western blot showing cleaved-caspase-1 (C and D) and caspase-1 (C and E) levels in the kidneys of control and OXO/adenine-induced mice (n = 5 animals per group). Western blot showing RIG-I (C and F) levels in the kidneys of control and OXO/adenine-induced mice (n = 5 animals per group).

(G–I) Representative fluorescence microscopy images of normal renal tissue stained for AQP-1, RIG-I and caspase-1 to identify the colocalization of caspase-1 and RIG-I in renal tubules. Scale bar 50 μm.

(J) Co-IP assay results showing the interplay between RIG-I and caspase-1 in NRK-52E cells treated with UA for 48 h. Data for (D–F) are presented as mean ± SEM. One-way ANOVA with Student-Newman-Keuls test for (D–F).

Norm-diet, normal diet. UA, uric acid.

See also Figure S1.

evidenced by western blot analysis (Figures 4I–4K). Additionally, ELISA results demonstrated that the levels of IL-1β in the culture medium mirrored the findings of the pre-animal experiment (Figure 4L). In addition, western blot results showed that the UA-induced increase in fibrosis marker levels (α-SMA, fibronectin and E-cadherin) was inhibited by knockdown of GSDMD expression (Figures 4M–4P).

RIG-I-siRNA decreased HUA-induced fibrosis and pyroptosis molecules expressions in NRK-52E cells *in vitro*

To further investigate the role of RIG-I in HN, NRK-52E cells were transfected with RIG-I-specific siRNA or NC-siRNA and then treated with uric acid. Western blot results showed that the expressions of RIG-I, caspase-1, GSDMD, cleaved-caspase-1 and GSDMD-N were raised after UA treatment in cell lysates. What's more, these increases were reduced via knocking down RIG-I expression using siRNA (Figures 5A–5G). The results of ELISA showed that a significant increase in the concentration of IL-1β in the culture medium after UA treatment. The increase in IL-1β production was eliminated by inhibition of RIG-I expression by siRNA (Figure 5H).

Western blot analysis of fibronectin and α-SMA expression showed that fibrosis occurred in UA-treated NRK-52E cells. Furthermore, knockdown of RIG-I expression substantially diluted the increase in fibronectin and α-SMA levels after UA treatment (Figures 5I–5K).

Caspase-1 siRNA reduced pyroptosis *in vitro*

Caspase-1 is an essential molecule in the pyroptosis pathway, and caspase-1-specific siRNA was used to examine pyroptosis in UA-treated NRK-52E cells and the relationship between RIG-I and caspase-1. Knocking down caspase-1 expression using siRNA significantly attenuated the UA-induced increases in pyroptosis-related protein levels, including caspase-1, cleaved-caspase-1, GSDMD and GSDMD-N. In contrast, the western blot results showed that caspase-1-siRNA had no effect on UA-induced expression of RIG-I (Figures 6A–6G). The ELISA results showed that knocking down caspase-1 expression abrogated the raise in IL-1β in the culture medium (Figure 6H).

RIG-I overexpression raised caspase-1 activity

To address role of RIG-I in caspase-1 activation, we examined the consequence of overexpressing RIG-I. We found that RIG-I overexpression in NRK-52E cells promoted caspase-1 cleavage to its active caspase-1 (Figures 7A–7D). And it also promoted pro-IL-1β protein express and cleaved-IL-1β protein release (Figures 7E and 7F). IL-1β production also increased in the culture medium after RIG-I overexpression (Figure 7G). In addition, RIG-I overexpression exhibited raise caspase-1 activity (Figure 7H). To further define this relationship, we knockdown caspase-1 expression then examined the consequence of overexpressing RIG-I. We found caspase-1 siRNA lower IL-1β production and caspase-1 activity in response to RIG-I overexpression (Figures 7I–7M). Collectively, these data suggest RIG-I overexpression triggers pyroptosis through activation of caspase-1.

DISCUSSION

HUA has become an independent risk factor for CKD, which causes HN. Considerable efforts have been made in past years, but the exact mechanism by which HUA induces CKD has not been fully elucidated.[17,18] It is now widely accepted that the development of CKD is mainly characterized by fibrosis, which is a comprehensive consequence of injuries.[19,20] Numerous studies have identified several cytokines that trigger fibrosis, with pro-inflammatory factors such as IL-18 and IL-1β strongly associated with various chronic diseases.[21] Renal tubules play a significant role in CKD progression, as tubular epithelial cells undergo changes and act as inflammatory and fibrogenic cells. The role of GSDMD in cytokine release and pyroptosis has been identified, suggesting a vital role in controlling the progression of hyperuricemic nephropathy. In our study, we displayed that GSDMD deficiency attenuated the renal injury in a murine HN model (Figure 1). Knocking down GSDMD reduced uric acid-induced damage to tubular epithelial cells (Figure 2).

Initial pyroptosis researches focused on immune-related cells such as macrophages. To explore the function of gasdermins in other tissues and cell types, a large number of studies have been conducted and verified that pyroptosis is not limited to phagocytes. We also observed the expression of GSDMD in the primary renal tubules (Figure S1). It is currently recognized that inhibiting pyroptosis can significantly alleviate kidney injury and protect from tubular necrosis. Miao et al. detected the fragmentation of GSDMD through western blot analysis of whole kidney lysates in cisplatin induced and ischemia-reperfusion induced acute kidney injury (AKI) models.[22] Knockouts of caspase-11 or GSDMD significantly protected mice from cisplatin induced AKI. Wang et al. found that TLR4/NF-κB and GSDMD-N expression were

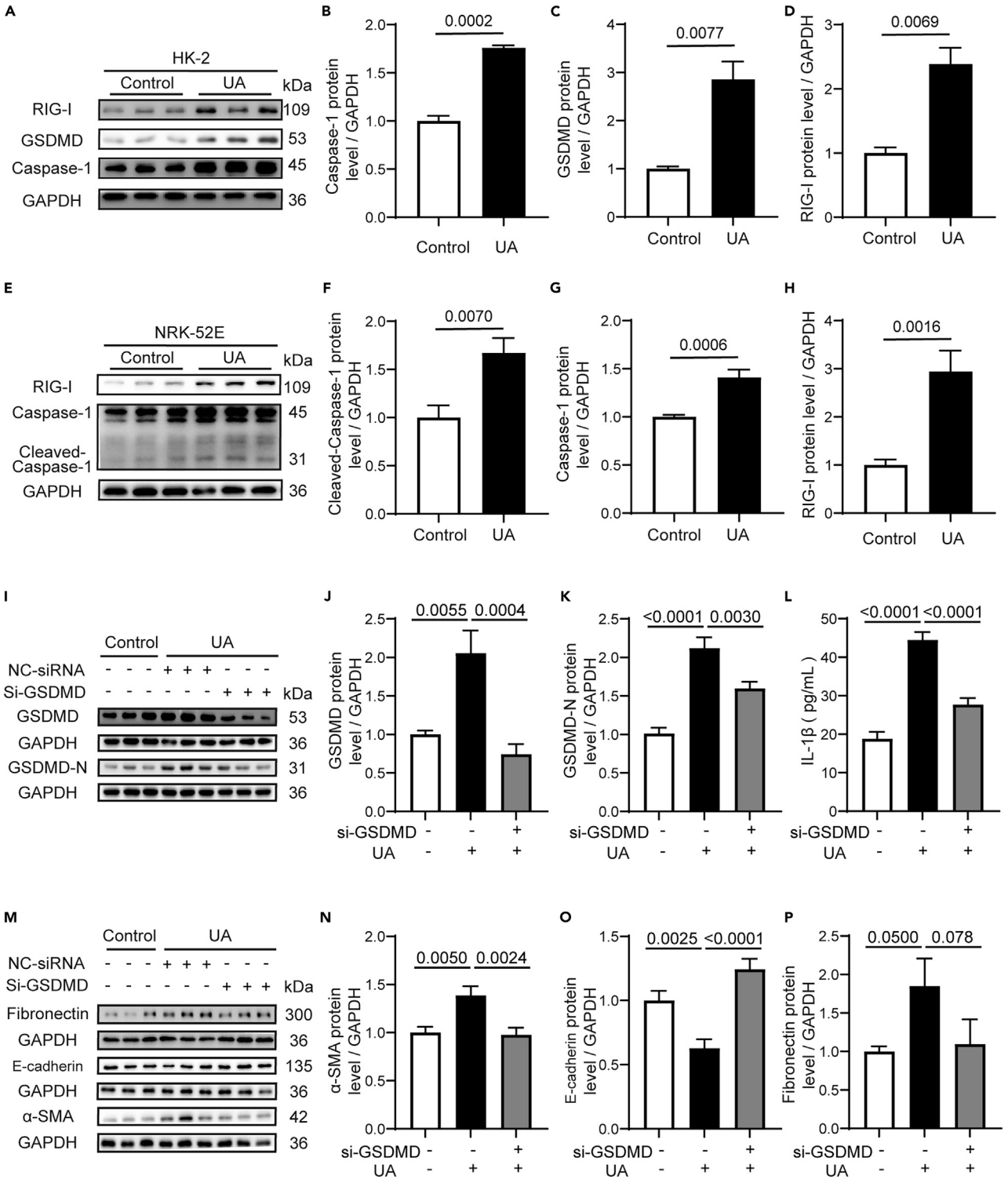

Figure 4. GSDMD encouraged IL-1β expression and fibrosis in NRK-52E cells in vitro

(A–D) HK-2 cells were stimulated with uric acid for 48 h. Western blot showing caspase-1 (A and B), GSDMD (A and C) and RIG-I (A and D) levels in HK-2 cells in the different groups (n = 3 per group).

(E–H) NRK-52E cells were stimulated with uric acid for 48 h. Western blot showing cleaved-caspase-1 (E and F), caspase-1 (E and G) and RIG-I (E and H) levels in NRK-52E cells in the different group (n = 6 per group).

Figure 4. *Continued*

(I–P) NRK-52E cells were transfected with GSDMD-siRNA or NC-siRNA and treated with UA for 48 h. Western blot showing GSDMD (I and J) and GSDMD-N (I and K) levels after UA treatment with or without GSDMD knockdown (n = 6 per group).

(L) IL-1β level in culture medium (n = 6 per group).

(M–P) Western blot showing α-SMA (M and N), E-cadherin (M and O) and fibronectin (M and P) levels after UA treatment with or without GSDMD knockdown (n = 6 per group).

Data for (B–D), (F–H), (J–L) and (N–P) are presented as mean ± SEM. Student's *t* test for (B–D) and (F–H). One-way ANOVA with Student-Newman-Keuls test for (J–L) and (N–P).

UA, uric acid.

increased in HK-2 cells in a hyperglycemic environment, and inhibition of TLR4/NF-κB signaling mitigated caspase-1/GSDMD-mediated renal tubular cell pyroptosis.[23]

Although inhibition of pyroptosis can significantly alleviate renal fibrosis, the role of bone marrow-derived cells or renal parenchymal cells in renal fibrosis remains a controversial issue. In the mouse model of renal fibrosis caused by unilateral ureteral obstruction (UUO), bone marrow transplantation technology was used to confirm that renal parenchymal cells, but not hematopoietic cells, are involved in renal fibrosis. Amplified inflammatory responses in renal tubular cells play an important role in the process of renal fibrosis.[24] Intriguingly, a study published in 2022 confirmed that GSDMD expressed in different immune cells is involved in UUO model induced-renal fibrosis.[25] In the UUO mouse model, there is a large infiltration of neutrophils and macrophage inflammatory cells in the obstructed kidney.[26] In contrast of the acute kidney damage caused by unilateral renal ureteral ligation, our inquiry is uric acid-induced CKD. Uric acid is the end-product of purine metabolism in humans and an intermediary product in most other mammals. Uric acid itself is nontoxic and harmless to the body, and kidney plays a key role in the regulation of uric acid homeostasis.[27,28]

The proximal renal tubules contain uric acid transporters, including transporters that assist in uric acid excretion, and transporters that assist in uric acid reabsorption.[29,30] Thus, under the condition of high uric acid, the proximal tubules of the kidney are the main targets of uric acid attack. Uric acid can affect the morphology and dysfunction of renal tubular epithelial cells by activating the NLRP3 inflammasome and secreting related inflammatory factors.[31,32] Activation of NLRP3 in renal tubular epithelial cells exacerbates the inflammatory response and subsequent renal fibrosis.[33] Although our research in NRK-52E cells suggests that GSDMD regulates renal tubular cell pyroptosis and alleviates uric acid induced renal fibrosis (Figure 4), we do not rule out the role of bone marrow-derived cells. To overcome this limitation, using bone marrow transplantation and renal tubular cell-specific GSDMD knockout mice are needed in the future.

The initiation of pyroptosis can be traced back to DAMPs and pathogen-associated molecular patterns (PAMPs).[34] When cells recognize DAMPs and PAMPs, PRRs is activated. Activated PRRs such as AIM2 and NLRP3 induce the formation of homotypic pyrin domain filaments with ASCs. As a bridge adaptor, ASC exposes the CARDs to recruit caspase family through CARD-CARD homotypic interactions.[35] However, it has also been shown that activation of the caspase family does not depend on the CARD structural domain of ASC. Additional studies have confirmed some inflammasomes can elicit specific caspase-1 signals in ASC-deficient cells. For example, the NLRC4 inflammasome directly recruits caspase-1 to trigger pyroptosis in ASC-deficient macrophages.[36] And ASC-driven caspase-1 auto-processing and speck formation are dispensable for the activation of caspase-1 and the NLRP1b inflammasome.[37] Kim et al. co-transfected Flag-RIG-I and Pro-caspase-1-V5 into HepG2 cells and detected RIG-I in supernatant of pro-caspase-1 transfected cells, along with caspase-1.[13] New research in 2022 showed that polarization and pyroptosis might be mediated by the RIG-I/caspase-1/GSDMD signaling pathway caused by crush syndrome.[38]

Our study found an upregulation of caspase-1 activity after RIG-I overexpression (Figure 7). Co-IP results showed that RIG-I and caspase-1 interacted at the protein level (Figure 3J), suggesting that uric acid may activate caspase-1 through RIG-I. Since RIG-I was discovered, multiple studies have focused on its role in viral recognition, and it is currently believed that its molecular structure contains a pair of CARD structures, and the release of CARDs is the first step to complete the activation of RIG-I signals.[39] We speculate that RIG-I activates caspase-1 through CARD-CARD interactions. In future investigations, we will further focus on RIG-I and caspase-1 binding sites.

RIG-I expression site is another area of concern. We observed RIG-I expresses in the nucleus of tubular cell. In recent study, the nucleus component of RIG exerts sensing ability when the viral agonists are exported by nucleus. Liu et al. found that nucleus RIG-I recognizes and binds to the ribonucleic acid of IAV and activates the interferon response.[40] RIG-I also had reported that it accumulated in the nucleus of macrophages and fibroblasts after virus infection.[41] Meanwhile, common pathogen-associated molecules are recognized by RIG-I in several cellular compartments of immune cells and nonimmune cells inside the kidney.[42] In lupus nephritis, RIG-I hyperactivation, which caused by DDX58 R109C variant, increased MAVS aggregation and caused kidney damage.[43] Therefore, the role of RIG-I in renal injury deserves to be further explored.

Table 2. The siRNA interference sequences

siRNA name	Target sequences
Caspase-1	GGGCAAGCCAGATGTTTAT
RIG-I	CCATGCTGCACATCTGCAA
GSDMD	GTCAAGTCTAGGCCAGAAA

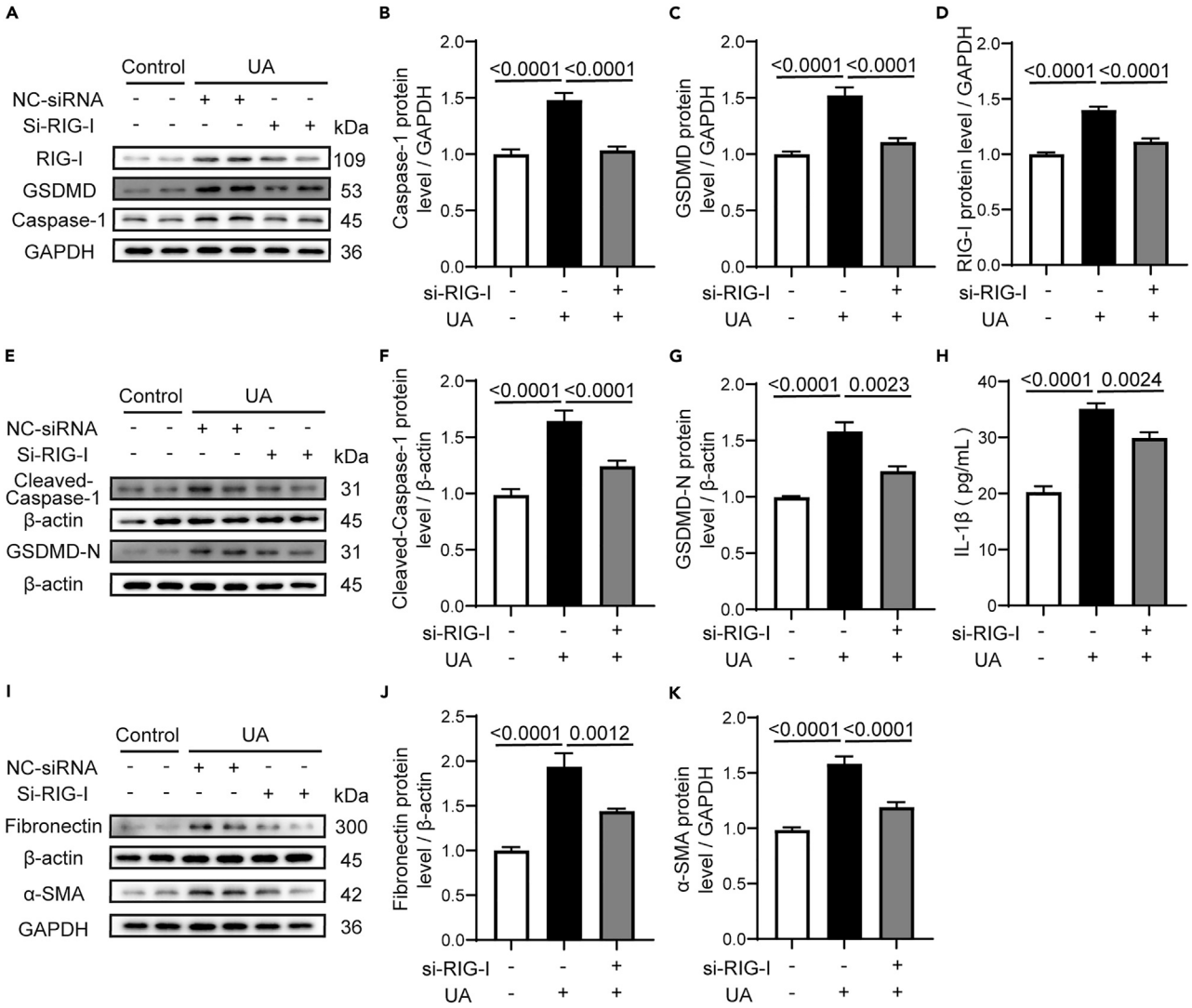

Figure 5. RIG-I-siRNA decreased HUA-induced fibrosis and pyroptosis molecules expressions in NRK-52E cells in vitro

NRK-52E cells were transfected with RIG-I-siRNA or NC-siRNA and treated with UA for 48 h.

(A–D) Western blot showing caspase-1 (A and B), GSDMD (A and C) and RIG-I (A and D) expressions after UA treatment with or without RIG-I knockdown (n = 6 per group).

(E–G) Western blot showing cleaved-caspase-1 (E and F) and GSDMD-N (E and G) expressions after UA treatment with or without RIG-I knockdown (n = 6 per group).

(H) IL-1β level in culture medium (n = 6 per group).

(I–K) Western blot showing fibronectin (I and J) and α-SMA (I and K) expressions after UA treatment with or without RIG-I knockdown (n = 6 per group).

Data for (B–D), (F–H) and (J–K) are presented as mean ± SEM. One-way ANOVA with Student-Newman-Keuls test for (B–D), (F–H) and (J–K).

UA, uric acid.

In summary, our results found that genetic knockout GSDMD significantly improved renal function after HN. We provide mechanistic insights into high urate causes damage to renal tubular epithelial cells, and RIG-I regulates GSDMD via caspase-1 to trigger proptosis. We anticipate that our studies may be broadly applicable to renal protective therapy, specifically targeting GSDMD for reduced renal fibrosis after HN.

Limitations of the study

Although our study showed that GSDMD promotes HUA -induced renal injury through RIG-I/caspase-1 pathway, future studies need to address the role of renal tubular epithelial cell-derived GSDMD in hyperuricemia-induced renal damage through renal tubular epithelial cell-specific GSDMD knockout mice. In addition, the mechanism by which RIG regulates caspase-1 is still unclear.

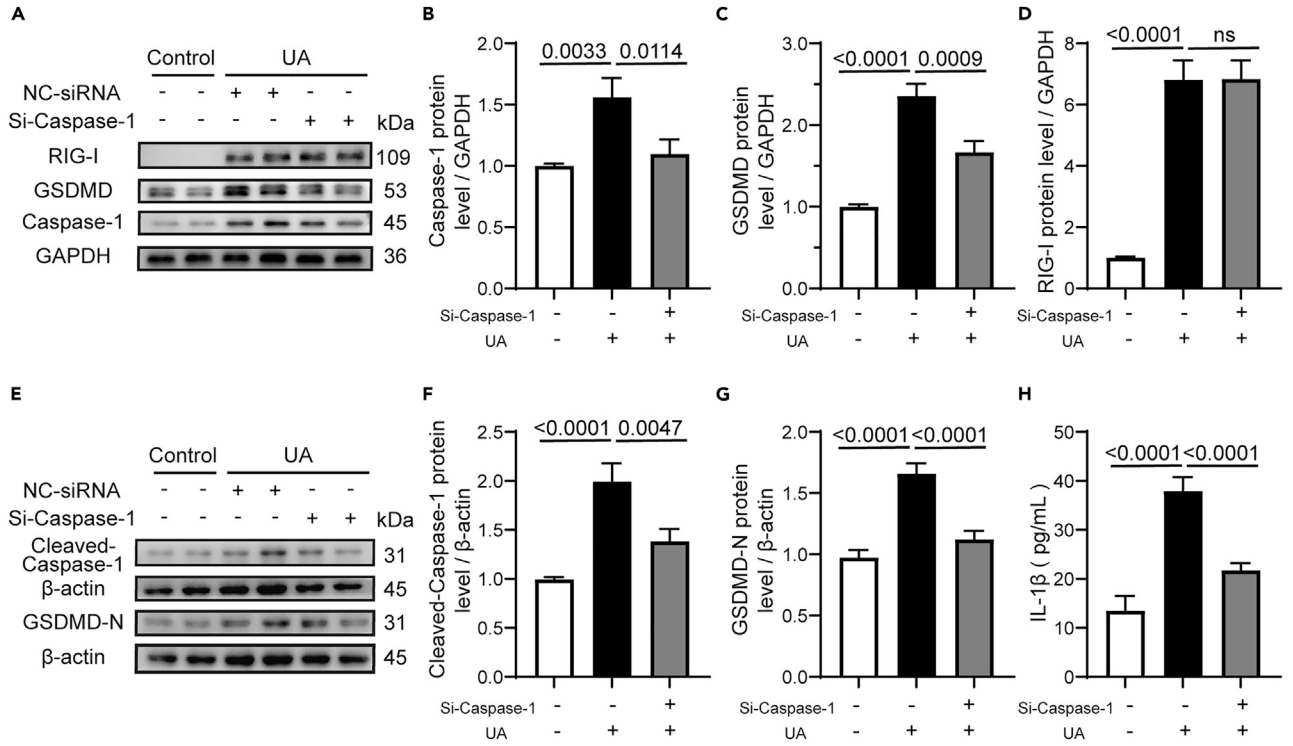

Figure 6. Caspase-1 siRNA had no effect on HUA-induced RIG-I expression but reduced pyroptosis *in vitro*

NRK-52E cells were transfected with caspase-1-siRNA or NC-siRNA and treated with UA for 48 h.

(A–D) Western blot showing caspase-1 (A and B), GSDMD (A and C) and RIG-I (A and D) levels after UA treatment with or without caspase-1 knockdown (n = 6 per group).

(E–G) Western blot showing cleaved-caspase-1 (E and F) and GSDMD-N (E and G) levels after UA treatment with or without caspase-1 knockdown (n = 6 per group).

(H) IL-1β level in culture medium (n = 6 per group).

Data for (B–D) and (F–H) are presented as mean ± SEM. One-way ANOVA with Student-Newman-Keuls test for (B–D) and (F–H).

UA, uric acid.

STAR★METHODS

Detailed methods are provided in the online version of this paper and include the following:

- KEY RESOURCES TABLE
- RESOURCE AVAILABILITY
  - Lead contact
  - Materials availability
  - Data and code availability
- EXPERIMENTAL MODEL AND STUDY PARTICIPANT DETAILS
  - Animals
  - Cell culture
- METHOD DETAILS
  - Materials
  - Renal histology
  - Immunofluorescence analysis
  - Blood examinations
  - Quantitative RT–PCR
  - Western blotting
  - ELISA assay
  - Co-immunoprecipitation assay
  - Caspase-1-, RIG-I- and GSDMD-specific siRNAs

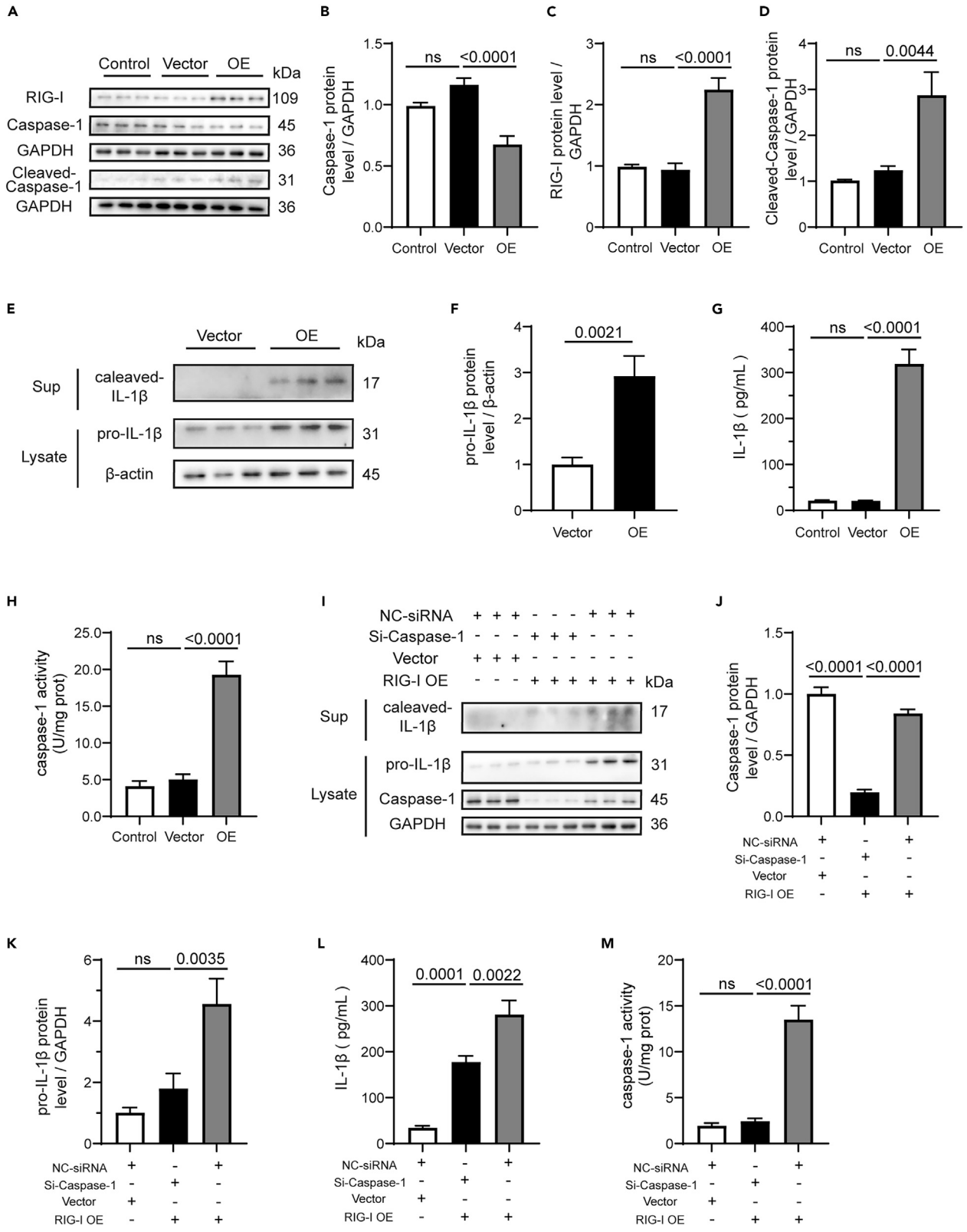
A
Control
Vector
OE
kDa
RIG-I
109
Caspase-1
45
GAPDH
36
Cleaved-Caspase-1
31
GAPDH
36
B
Caspase-1 protein level / GAPDH
ns
<0.0001
Control
Vector
OE
C
RIG-I protein level / GAPDH
ns
<0.0001
Control
Vector
OE
D
Cleaved-Caspase-1 protein level / GAPDH
ns
0.0044
Control
Vector
OE
E
Vector
OE
kDa
Sup
caleaved-IL-1β
17
Lysate
pro-IL-1β
31
β-actin
45
F
pro-IL-1β protein level / β-actin
0.0021
Vector
OE
G
IL-1β (pg/mL)
ns
<0.0001
Control
Vector
OE
H
caspase-1 activity (U/mg prot)
ns
<0.0001
Control
Vector
OE
I
NC-siRNA
Si-Caspase-1
Vector
RIG-I OE
kDa
Sup
caleaved-IL-1β
17
Lysate
pro-IL-1β
31
Caspase-1
45
GAPDH
36
J
Caspase-1 protein level / GAPDH
<0.0001
<0.0001
NC-siRNA
Si-Caspase-1
Vector
RIG-I OE
K
pro-IL-1β protein level / GAPDH
ns
0.0035
NC-siRNA
Si-Caspase-1
Vector
RIG-I OE
L
IL-1β (pg/mL)
0.0001
0.0022
NC-siRNA
Si-Caspase-1
Vector
RIG-I OE
M
caspase-1 activity (U/mg prot)
ns
<0.0001
NC-siRNA
Si-Caspase-1
Vector
RIG-I OE

Figure 7. RIG-I overexpression raised caspase-1 activity

(A–F) NRK-52E cells were transfected with vector or RIG-I plasmid (OE), then the cell lysates and culture supernatants (Sup) were collected and immunoblotted with the indicated antibodies. Western blot showing caspase-1 (A and B) RIG-I (A and C) and cleaved-caspase-1 (A and D) levels (n = 6 per group); pro-IL-1β (E and F, n = 6 per group).

(G) ELISA analysis of IL-1β from the cell-free supernatant of cells treated as states in A (n = 6 per group).

(H) Activity analysis of caspase-1 from the cells which digested with pancreatic enzymes and treated as states in A (n = 6 per group).

(I–K) NRK-52E cells were transfected with NC-siRNA or Si-Caspase-1. These cells were transfected with vector or RIG-I plasmid (OE), then the cell lysates and culture supernatants (Sup) were collected and immunoblotted with the indicated antibodies. Western blot showing caspase-1 (I and J) and pro-IL-1β (I and K) levels (n = 6 per group).

(L) ELISA analysis of IL-1β from the cell-free supernatant of cells treated as states in I (n = 6 per group).

(M) Activity analysis of caspase-1 from the cells which digested with pancreatic enzymes and treated as states in I (n = 6 per group).

Data for (B–D), (F–H) and (J–M) are presented as mean ± SEM. Student's *t* test for (F). One-way ANOVA with Student-Newman-Keuls test for (B–D), (G–H) and (J–M).

Sup, supernatants. OE, overexpression.

SUPPLEMENTAL INFORMATION

Supplemental information can be found online at https://doi.org/10.1016/j.isci.2023.108463.

ACKNOWLEDGMENTS

Thanks to Professor Limin Lu (Fudan University) for providing transgenic mice. Thanks to researcher Naijun Miao (Shanghai Jiao Tong University) for providing RIG-I plasmids. The work was supported by National Natural Science Foundation of China (No. 81400695), Anhui Provincial Natural Science Foundation (No. 1508085QH153 & 1908085QC132) and Natural Science Foundation of Higher Education Institutions (No. 2022AH040173).

AUTHOR CONTRIBUTIONS

D.C.S. and L.S.M. designed the research, analyzed data, wrote the first draft, and revised the manuscript. L.S.M., R.Q.S., J.J., X.D.L., and B.Z. were involved in the research. A.P.X., H.L., and L.M.L. contributed new reagents, analytic tools, and transgenic mice. D.C.S. supervised the research. All authors reviewed and edited the draft.

DECLARATION OF INTERESTS

All authors declare no competing interests.

Received: February 23, 2023
Revised: October 10, 2023
Accepted: November 13, 2023
Published: November 14, 2023

REFERENCES

1. Ponticelli, C., Podestà, M.A., and Moroni, G. (2020). Hyperuricemia as a trigger of immune response in hypertension and chronic kidney disease. Kidney Int. *98*, 1149–1159.
2. Brien, M.E., Duval, C., Palacios, J., Boufaied, I., Hudon-Thibeault, A.A., Nadeau-Vallée, M., Vaillancourt, C., Sibley, C.P., Abrahams, V.M., Jones, R.L., and Girard, S. (2017). Uric Acid Crystals Induce Placental Inflammation and Alter Trophoblast Function via an IL-1-Dependent Pathway: Implications for Fetal Growth Restriction. J. Immunol. *198*, 443–451.
3. Hu, Y., Shi, Y., Chen, H., Tao, M., Zhou, X., Li, J., Ma, X., Wang, Y., and Liu, N. (2022). Blockade of Autophagy Prevents the Progression of Hyperuricemic Nephropathy Through Inhibiting NLRP3 Inflammasome-Mediated Pyroptosis. Front. Immunol. *13*, 858494.
4. Wan, J., Liu, D., Pan, S., Zhou, S., and Liu, Z. (2022). NLRP3-mediated pyroptosis in diabetic nephropathy. Front. Pharmacol. *13*, 998574.
5. Bai, C., Zhu, Y., Dong, Q., and Zhang, Y. (2022). Chronic intermittent hypoxia induces the pyroptosis of renal tubular epithelial cells by activating the NLRP3 inflammasome. Bioengineered *13*, 7528–7540.
6. Ding, J., Wang, K., Liu, W., She, Y., Sun, Q., Shi, J., Sun, H., Wang, D.C., and Shao, F. (2016). Pore-forming activity and structural autoinhibition of the gasdermin family. Nature *535*, 111–116.
7. Fernandes-Alnemri, T., Yu, J.W., Datta, P., Wu, J., and Alnemri, E.S. (2009). AIM2 activates the inflammasome and cell death in response to cytoplasmic DNA. Nature *458*, 509–513.
8. Hornung, V., Ablasser, A., Charrel-Dennis, M., Bauernfeind, F., Horvath, G., Caffrey, D.R., Latz, E., and Fitzgerald, K.A. (2009). AIM2 recognizes cytosolic dsDNA and forms a caspase-1-activating inflammasome with ASC. Nature *458*, 514–518.
9. Poyet, J.L., Srinivasula, S.M., Tnani, M., Razmara, M., Fernandes-Alnemri, T., and Alnemri, E.S. (2001). Identification of Ipaf, a human caspase-1-activating protein related to Apaf-1. J. Biol. Chem. *276*, 28309–28313.
10. Thoresen, D., Wang, W., Galls, D., Guo, R., Xu, L., and Pyle, A.M. (2021). The molecular mechanism of RIG-I activation and signaling. Immunol. Rev. *304*, 154–168.

11. Iurescia, S., Fioretti, D., and Rinaldi, M. (2020). The Innate Immune Signalling Pathways: Turning RIG-I Sensor Activation against Cancer. Cancers *12*, 3158.
12. Xu, S., Jin, T., and Weng, J. (2022). Endothelial Cells as a Key Cell Type for Innate Immunity: A Focused Review on RIG-I Signaling Pathway. Front. Immunol. *13*, 951614.
13. Kim, M.J., and Yoo, J.Y. (2008). Active caspase-1-mediated secretion of retinoic acid inducible gene-I. J. Immunol. *181*, 7324–7331.
14. Hu, J., He, Y., Yan, M., Zhu, C., Ye, W., Zhu, H., Chen, W., Zhang, C., and Zhang, Z. (2013). Dose dependent activation of retinoic acid-inducible gene-I promotes both proliferation and apoptosis signals in human head and neck squamous cell carcinoma. PLoS One *8*, e58273.
15. Wang, P.T., Li, N., Wang, X.Y., Chen, J.L., Geng, C.H., Liu, Z.Q., Fan, H.J., Lv, Q., Hou, S.K., and Gong, Y.H. (2021). RIG-I, a novel DAMPs sensor for myoglobin activates NF-kappaB/caspase-3 signaling in CS-AKI model. Mil. Med. Res. *8*, 37.
16. Poeck, H., Bscheider, M., Gross, O., Finger, K., Roth, S., Rebsamen, M., Hannesschläger, N., Schlee, M., Rothenfusser, S., Barchet, W., et al. (2010). Recognition of RNA virus by RIG-I results in activation of CARD9 and inflammasome signaling for interleukin 1 beta production. Nat. Immunol. *11*, 63–69.
17. Matsuo, H., Ishikawa, E., Machida, H., Mizutani, Y., Tanoue, A., Ohnishi, T., Murata, T., Okamoto, S., Ogura, T., Nishimura, Y., et al. (2020). Efficacy of xanthine oxidase inhibitor for chronic kidney disease patients with hyperuricemia. Clin. Exp. Nephrol. *24*, 307–313.
18. Kataoka, H., Mochizuki, T., Ohara, M., Tsuruta, Y., Iwasa, N., Yoshida, R., Tsuchiya, K., Nitta, K., Kimura, K., and Hosoya, T.; FEATHER Investigators (2022). Urate-lowering therapy for CKD patients with asymptomatic hyperuricemia without proteinuria elucidated by attribute-based research in the FEATHER Study. Sci. Rep. *12*, 3784.
19. Liu, B.C., Tang, T.T., Lv, L.L., and Lan, H.Y. (2018). Renal tubule injury: a driving force toward chronic kidney disease. Kidney Int. *93*, 568–579.
20. Djudjaj, S., and Boor, P. (2019). Cellular and molecular mechanisms of kidney fibrosis. Mol. Aspect. Med. *65*, 16–36.
21. Xu, B., Jiang, M., Chu, Y., Wang, W., Chen, D., Li, X., Zhang, Z., Zhang, D., Fan, D., Nie, Y., et al. (2018). Gasdermin D plays a key role as a pyroptosis executor of non-alcoholic steatohepatitis in humans and mice. J. Hepatol. *68*, 773–782.
22. Miao, N., Yin, F., Xie, H., Wang, Y., Xu, Y., Shen, Y., Xu, D., Yin, J., Wang, B., Zhou, Z., et al. (2019). The cleavage of gasdermin D by caspase-11 promotes tubular epithelial cell pyroptosis and urinary IL-18 excretion in acute kidney injury. Kidney Int. *96*, 1105–1120.
23. Wang, Y., Zhu, X., Yuan, S., Wen, S., Liu, X., Wang, C., Qu, Z., Li, J., Liu, H., Sun, L., and Liu, F. (2019). TLR4/NF-κB Signaling Induces GSDMD-Related Pyroptosis in Tubular Cells in Diabetic Kidney Disease. Front. Endocrinol. *10*, 603.
24. Li, Y., Yuan, Y., Huang, Z.X., Chen, H., Lan, R., Wang, Z., Lai, K., Chen, H., Chen, Z., Zou, Z., et al. (2021). GSDME-mediated pyroptosis promotes inflammation and fibrosis in obstructive nephropathy. Cell Death Differ. *28*, 2333–2350.
25. Wang, Y., Li, Y., Chen, Z., Yuan, Y., Su, Q., Ye, K., Chen, C., Li, G., Song, Y., Chen, H., and Xu, Y. (2022). GSDMD-dependent neutrophil extracellular traps promote macrophage-to-myofibroblast transition and renal fibrosis in obstructive nephropathy. Cell Death Dis. *13*, 693.
26. Kim, J., Imig, J.D., Yang, J., Hammock, B.D., and Padanilam, B.J. (2014). Inhibition of soluble epoxide hydrolase prevents renal interstitial fibrosis and inflammation. Am. J. Physiol. Ren. Physiol. *307*, F971–F980.
27. Xu, X., Li, C., Zhou, P., and Jiang, T. (2016). Uric acid transporters hiding in the intestine. Pharm. Biol. *54*, 3151–3155.
28. Jalal, D.I., Chonchol, M., Chen, W., and Targher, G. (2013). Uric acid as a target of therapy in CKD. Am. J. Kidney Dis. *61*, 134–146.
29. Mallat, S.G., Al Kattar, S., Tanios, B.Y., and Jurjus, A. (2016). Hyperuricemia, Hypertension, and Chronic Kidney Disease: an Emerging Association. Curr. Hypertens. Rep. *18*, 74.
30. Chung, S., and Kim, G.H. (2021). Urate Transporters in the Kidney: What Clinicians Need to Know. Electrolyte & blood pressure. E & BP *19*, 1–9.
31. Zhou, F., Yu, G., Wang, G., Liu, Y., Zhang, L., Wang, W., and Chen, N. (2019). Association of serum uric acid levels with the incident of kidney disease and rapid eGFR decline in Chinese individuals with eGFR > 60 mL/min/1.73 m(2) and negative proteinuria. Clin. Exp. Nephrol. *23*, 871–879.
32. Wang, M., Lin, X., Yang, X., and Yang, Y. (2022). Research progress on related mechanisms of uric acid activating NLRP3 inflammasome in chronic kidney disease. Ren. Fail. *44*, 615–624.
33. Wang, W., Wang, X., Chun, J., Vilaysane, A., Clark, S., French, G., Bracey, N.A., Trpkov, K., Bonni, S., Duff, H.J., et al. (2013). Inflammasome-independent NLRP3 augments TGF-β signaling in kidney epithelium. J. Immunol. *190*, 1239–1249.
34. Broz, P., and Dixit, V.M. (2016). Inflammasomes: mechanism of assembly, regulation and signalling. Nat. Rev. Immunol. *16*, 407–420.
35. Liu, Z., Wang, C., Yang, J., Chen, Y., Zhou, B., Abbott, D.W., and Xiao, T.S. (2020). Caspase-1 Engages Full-Length Gasdermin D through Two Distinct Interfaces That Mediate Caspase Recruitment and Substrate Cleavage. Immunity *53*, 106–114.e5.
36. Broz, P., von Moltke, J., Jones, J.W., Vance, R.E., and Monack, D.M. (2010). Differential requirement for Caspase-1 autoproteolysis in pathogen-induced cell death and cytokine processing. Cell host & microbe *8*, 471–483.
37. Van Opdenbosch, N., Gurung, P., Vande Walle, L., Fossoul, A., Kanneganti, T.D., and Lamkanfi, M. (2014). Activation of the NLRP1b inflammasome independently of ASC-mediated caspase-1 autoproteolysis and speck formation. Nat. Commun. *5*, 3209.
38. Li, N., Chen, J., Geng, C., Wang, X., Wang, Y., Sun, N., Wang, P., Han, L., Li, Z., Fan, H., et al. (2022). Myoglobin promotes macrophage polarization to M1 type and pyroptosis via the RIG-I/Caspase1/GSDMD signaling pathway in CS-AKI. Cell Death Dis. *8*, 90.
39. Onomoto, K., Onoguchi, K., and Yoneyama, M. (2021). Regulation of RIG-I-like receptor-mediated signaling: interaction between host and viral factors. Cell. Mol. Immunol. *18*, 539–555.
40. Liu, G., Lu, Y., Thulasi Raman, S.N., Xu, F., Wu, Q., Li, Z., Brownlie, R., Liu, Q., and Zhou, Y. (2018). Nuclear-resident RIG-I senses viral replication inducing antiviral immunity. Nat. Commun. *9*, 3199.
41. Wang, C., Zhou, W., Liu, Y., Xu, Y., Zhang, X., Jiang, C., Jiang, M., and Cao, X. (2022). Nuclear translocation of RIG-I promotes cellular apoptosis. J. Autoimmun. *130*, 102840.
42. Anders, H.J. (2007). Innate pathogen recognition in the kidney: toll-like receptors, NOD-like receptors, and RIG-like helicases. Kidney Int. *72*, 1051–1056.
43. Peng, J., Wang, Y., Han, X., Zhang, C., Chen, X., Jin, Y., Yang, Z., An, Y., Zhang, J., Liu, Z., et al. (2023). Clinical Implications of a New DDX58 Pathogenic Variant That Causes Lupus Nephritis due to RIG-I Hyperactivation. J. Am. Soc. Nephrol. *34*, 258–272.

STAR★METHODS

KEY RESOURCES TABLE

REAGENT or RESOURCE	SOURCE	IDENTIFIER
Antibodies		
Anti-RIG-I antibody	Cell Signaling Technology	Cat# 3743; RRID: AB_2269233
Anti-Gasdermin D antibody	Cell Signaling Technology	Cat# 39754; RRID: AB_2916333
Anti-cleaved Gasdermin D antibody	Cell Signaling Technology	Cat# 36425; RRID: AB_2799099
Anti-caspase-1 antibody	Cell Signaling Technology	Cat# 24232; RRID: AB_2890194
Anti-cleaved Caspase-1 antibody	Cell Signaling Technology	Cat# 89332; RRID: AB_2923067
Anti- E-cadherin antibody	Cell Signaling Technology	Cat# 3195; RRID: AB_2291471
Anti-α-Smooth Muscle antibody	Cell Signaling Technology	Cat# 19245; RRID: AB_2734735
Anti-Fibronectin antibody	Cell Signaling Technology	Cat# 63779
Anti-Aquaporin 1 antibody	Santa Cruz Biotechnology	Cat# sc-25287; RRID: AB_626694
Anti-caspase-1 antibody	Santa Cruz Biotechnology	Cat# sc-392736; RRID: AB_2890615
Anti-RIG-I/DDX58 antibody	Abcam	Cat# ab302778
Anti-Aquaporin 1 antibody	Affinity Bioscience	Cat# AF5231; RRID: AB_2837717
Anti-mouse-IL-1β antibody	Gene Tex	Cat# GTX74034; RRID: AB_378141
Anti-GAPDH antibody	ABclonal Technology	Cat# AC001; RRID: AB_2619673
anti-β-actin antibody	ABclonal Technology	Cat# AC006; RRID: AB_2768236
HRP Goat Anti-Rabbit IgG (H+L)	ABclonal Technology	Cat# AS014; RRID: AB_2769854
HRP Goat Anti-Mouse IgG (H+L)	ABclonal Technology	Cat# AS003; RRID: AB_2769851
Alexa Fluor 555-labeled Donkey Anti-Rabbit IgG(H+L)	Beyotime BioTechnology	Cat# A0453; RRID: AB_2890132
Alexa Fluor 488-labeled Goat Anti-Mouse IgG(H+L)	Beyotime BioTechnology	Cat# A0428; RRID: AB_2893435
Chemicals, peptides, and recombinant proteins		
Potassium oxonate	Mackin	Cat# P831461
Adenine	Mackin	Cat# A800685
Carboxymethyl cellulose sodium	Mackin	Cat# C835846
TRIzol reagent	Invitrogen	Cat# 15596026
Uric acid	Sigma-Aldrich	Cat# U2625
Critical commercial assays		
Hematoxylin-Eosin (HE) Stain Kit	Solarbio	Cat# G1120
Masson's Trichrome Stain Kit	Solarbio	Cat# G1340
Caspase-1 Activity Assay Kit	Solarbio	Cat# BC3810-100T
riboFECT CP Transfection Kit (166T)	RiboBio	C10511-05
Lipofectamine 3000 Transfection Reagent	Invitrogen	Cat# L3000-015
Protein-A magnetic beads	Thermo Fisher Scientific	Cat# 88846
NovoStart®SYBR qPCR SuperMix Plus	Novoprotein	Cat# E096-01A
HyperScrlpt III RT SuperMix for qPCR with gDNA Remover	EnzyArtisan	Cat# R102
Uric acid (UA) Test Kit	NJJCBIO	Cat# C012-2-1
Creatinine (Cr) Assay kit (sarcosine oxidase)	NJJCBIO	Cat# C011-2-1
Mouse IL-1β Precoated ELISA Kit	Dakewe Biotech	Cat# 1210122

(*Continued on next page*)

Continued

REAGENT or RESOURCE	SOURCE	IDENTIFIER
RIPA lysis buffer	Beyotime BioTechnology	Cat# P0013B
Bradford protein assay kit	Beyotime BioTechnology	Cat# P0006
BCA protein assay kit	Beyotime BioTechnology	Cat# P0012
Deposited data		
GSDMD siRNA	RiboBio	Decribed in current manuscript
Caspase-1siRNA	RiboBio	Decribed in current manuscript
RIG-I siRNA	RiboBio	Decribed in current manuscript
Negative control siRNA	RiboBio	Decribed in current manuscript
Mouse GAPDH primer	Sango biotech	Decribed in current manuscript
Mouse Collagen I primer	Sango biotech	Decribed in current manuscript
Mouse Fibronectin primer	Sango biotech	Decribed in current manuscript
Mouse IL-1β primer	Sango biotech	Decribed in current manuscript
Experimental models: Cell lines		
NRK-52E	Procell Life Science & Technology	Cat# CL-0174
HK-2	Procell Life Science & Technology	Cat# CL-0109
Experimental models: Organisms/strains		
C57BL/6 mice	Henan Skbex Biotechnology	N/A
GSDMD$^{-/-}$ mice	Jackson Laboratory	Cat# 032663
Recombinant DNA		
RIG-I plasmids	Addgene	Cat# 160108
Software and algorithms		
Fluorescence microscope IX3	Olympus	https://www.olympus-lifescience.com
ABI PRISM 7000 HT	ABI	https://www.thermofisher.cn/us/en/home/brands/applied-biosystems.html
ImageJ	NIH	https://imagej.nih.gov/ij/index.html
GraphPad Prism v.9	GraphPad Software	https://www.graphpad.com/scientific-software/prism/
SPSS v.26	Analysis Software	https://www.ibm.com/cn-zh/spss

RESOURCE AVAILABILITY

Lead contact

Further information and requests for resources and reagents should be directed to and will be fulfilled by the Lead Contact, Decui Shao (shaodecui@wnmc.edu.cn).

Materials availability

The study did not generate new unique reagents.

Data and code availability

- All data reported in this paper will be shared by the lead contact upon request.
- This paper does not report original code.
- Any additional information required to reanalyze the data reported in this paper is avaliable from the lead contact upon request.

EXPERIMENTAL MODEL AND STUDY PARTICIPANT DETAILS

Animals

All animal experiments were agreed by the Laboratory Animal Welfare and Ethics Committee of Wannan Medical College, Wuhu, China (LLSC-2021-197). C57BL/6J WT mice (20 ±2 g) were used as wild-type mice. GSDMD$^{-/-}$ mice were provided by Limin Lu (Shanghai, China),

which contain a C57BL/6J genetic background. These mice were raised in a standard feeding environment with a 12-hour light/dark cycle and a temperature of 22 °C. Water and food are freely to get.

Both males and females were used. When the animals weight reached 20 ±2 g, the animals were separated into the WT-Norm-diet, WT-HUA, GSDMD$^{-/-}$-Norm-diet and GSDMD$^{-/-}$-HUA groups, randomly. Potassium oxonate (250 mg/kg/day) and adenine (50 mg/kg/day) melted in 2.5‰ carboxymethyl cellulose sodium (CMC-Na), administered the experimental mice by gavage to create the HUA model. An equivalent amount of CMC-Na was given to the control groups. After 28 days of intragastric administration, the mice were sacrificed.

Cell culture

The normal renal tubular epithelial NRK-52E cells and human proximal tubular tubular epithelial cells (HK-2) cells were purchased form Procell Life Science & Technology. NRK-52E cells were cultured in DMEM basic with 10% FBS and HK-2 cells were cultured in DMEM/F-12 basic with 10% FBS. Cells were left to standing overnight in medium containing 0.5% FBS before treated. Uric acid was melted in medium to an ultimate concentration of 0.15 g/L (0.9 mmol/L).

METHOD DETAILS

Materials

Anti-RIG-I (3743), anti-GSDMD (39754), anti-cleaved Gasdermin D (36425), anti-caspase-1 (24232), anti-cleaved caspase-1 (89332), anti-E-cadherin (3195), anti-FN (63779) and anti-α-SMA (19245) were provided by Cell Signaling Technology (Danvers, MA, USA). RIG-I/DDX58 antibody (ab302778) were obtained from Abcam (Cambridge, UK). AQP-1 rabbit antibody (AF5231) were obtained from Affinity Bioscience (Changzhou, China). AQP-1 mouse antibody (sc-25287) and caspase-1 mouse antibody (sc-392736) were obtained from Santa Cruz Biotechnology (Dallas, Texas, USA). Anti-mouse-IL-1β (74034) was purchased from GeneTex. Anti-GAPDH (AC001) and anti-β-actin (AC006) were provided by ABclonal Technology (Wuhan, China). Potassium oxonate, adenine and carboxymethyl cellulose sodium were provided by Mackin (Shanghai, China). Uric acid was provided by Sigma-Aldrich (USA). Dulbecco's Modified Eagle medium (DMEM) was provided by Gibco (Grand Island, NY, USA). Fetal bovine serum (FBS) was bought from Every Green (Hangzhou, China).

Renal histology

Renal samples were preserved, desiccated in graded alcohol series, embedded, and cut into slices about 5μm thickness. Hematoxylin and eosin (HE) staining was used to observe tissue morphologic changes. Tissue fibrosis was evaluated by Masson's trichrome staining.

Immunofluorescence analysis

Normal renal sections were immersed in citrate antigen retrieval solution at 95°C, and then used Triton X-100 to break the membrane. The sections were incubated with RIG-I, caspase-1 or AQP-1 antibodies at 4°C overnight after blocking treatment. The secondary antibody (Beyotime Biotechnology, Shanghai, China) was used to incubated at room temperature. PBS was used to wash the sections during this analysis. Fluorescence signals were viewed by a fluorescence microscope (IX3, Olympus, Japan).

Blood examinations

Blood was collected to measure serum uric acid and creatinine levels with a commercially available assay kit (NJJCBIO, Nanjing, China). Serum creatinine levels and urinary creatinine levels were measured.

Quantitative RT–PCR

Total RNA was extracted from renal tissue by TRIzol reagent (Invitrogen, USA). Reverse transcription into cDNA was performed by HyperScript III RT SuperMix for qPCR with gDNA Remover (EnzyArtisan, Shanghai, China). The qPCR system was prepared with a NovoStart®SYBR qPCR SuperMix Plus (Novoprotein, Shanghai, China). Then IL-1β, Fibronectin, Collagen I and GAPDH expression levels were measured using an ABI PRISM 7000 HT according to standard procedures. The $2^{-\triangle\triangle Ct}$ method was used to express the relative expression levels. The corresponding primer sequences are recorded in Table 1.

Western blotting

Cell samples and renal tissue samples were stored with a temperature of -80°C. All proteins of samples were extracted by RIPA lysis buffer (Beyotime, Shanghai, China). The proteins were separated by 8%-12% SDS–PAGE and transferred to polyvinylidene difluoride membranes. The membranes were incubated with specific primary antibodies overnight after blocking treatment. The secondary antibodies were incubating the membranes at room temperature to discern immunoreactive bands.

ELISA assay

After rinsing the tissue with pre-cooled PBS, the clipped tissue was added with an equivalent volume of PBS (1:9), mixed on ice and centrifuged at 5000 ×g for 10 min at 4°C. Tissue homogenate supernatants were collected and initially diluted to 1:3. Cell culture medium was

centrifuged at 1000 ×g for 10 min at 4°C, then the culture supernatants were collected and diluted to 1:3. IL-1β expression in tissues and cells was measured using commercially available ELISAs kits (Dakewe Bioengineering, Shenzhen, China).

Co-immunoprecipitation assay

To determine the interplay between caspase-1 and RIG-I, a Co-IP assay was conducted in NRK-52E cells. Total proteins were extracted from the control group (NC) and UA treatment group using RIPA lysis buffer, and incubated with 1 μg of caspase-1 antibody and 30 μL of protein-A magnetic beads (Thermo Fisher Scientific, USA) overnight with shaking. Caspase-1 and RIG-I antibodies were used for immunoblot analysis.

Caspase-1-, RIG-I- and GSDMD-specific siRNAs

To modify gene expression, caspase-1-, GSDMD-, and RIG-I-specific siRNAs were supplied by RiboBio (Guangzhou, Guangdong, China). RIG-I-specific siRNA (50 nmol/L), GSDMD-specific siRNA (50 nmol/L) and caspase-1-specific siRNA (50 nmol/L) or control siRNA (50 nmol/L) were transfected into NRK-52E with riboFECT CP Transfection Kit (RiboBio, Guangdong, China). The empty vector was used as control. Cells were left to standing overnight in medium embracing 0.5% FBS prior to being treated. The siRNA interference sequences are recorded in Table 2.

RIG-I overexpression and proteins enrichment by acetone

RIG-I plasmids were provided by Naijun Miao (Shanghai, China). 4 μg of RIG-I plasmids were transfected into NRK-52E cells using Lipofectamine 3000 Transfection Reagent (Invitrogen, USA) and the empty vector was used as the control. After 24 h, the cells were incubated in DMEM without FBS for 48 h. Caspase-1-specific siRNA transfection was performed prior to RIG-I overexpression. The culture medium is used on the one hand for the ELISA of IL-1β expression and on the other hand for protein enrichment by acetone. The serum-free culture treatment is designed to exclude the effect of serum proteins.

The culture medium was collected for enrich proteins with acetone. After pre-cooling the acetone at -20°C, the culture medium and the corresponding volume of acetone (1:4) were mixed thoroughly and stored at -80°C overnight. The next day, the samples were centrifuged at 10,000 r.p.m for 15 min at 4°C and the supernatant carefully discarded. Wait for the acetone to evaporate and dry, then bring up with 1 × sample buffer for SDS-PAGE.

Caspase-1 activity detection and bradford protein assay

Caspase-1 activity and protein levels were determined using caspase activity detection kit (Solarbio, Beijing, China) and the Bradford protein assay kit (Beyotime, Shanghai, China). All operations were performed strictly according to the manuals. Caspase-1 activity was determined by generating a PNA standard curve.

Isolation of mouse renal tubules

Renal cortexes were freshly isolated after harvesting the renal. Mice were anaesthetized by inhalation of ether. Then the laparotomy and bilateral nephrectomy were performed immediately. The kidneys were quickly removed and put into a 4°C Hank's balanced salt solution. After the renal capsule was removed, the cortex of kidney was separated and cut into small fragments and gently grinded. Then the suspension was filtered through a 100-μm strainer to separate glomeruli and get tubules. The filtrated tubule fragments were collected by centrifugation at 1000 × g at 4°C for 5 minutes.

QUANTIFICATION AND STATISTICAL ANALYSIS

Data are presented as mean ± SEM. In this study, we utilized GraphPad Prism and ImageJ software to draw column graphs and perform analysis for western bolt results. We utilized Student's t test to detect the differences between two groups. We utilized One-way ANOVA with Student-Newman-Keuls test to detect the differences among multiple groups. $p < 0.05$ was considered statistically significant.